J. Fluid Mech. (1998), *vol.* 364, *pp.* 297–318. Printed in the United Kingdom

Fine-scale structure of thin vortical layers

By TAKASHI ISHIHARA[1]† AND YUKIO KANEDA[2]

[1]Department of Mathematics, Faculty of Science, Toyama University, Gofuku, Toyama 930, Japan

[2]Department of Computational Science and Engineering, School of Engineering, Nagoya University, Chikusa-ku, Nagoya 464-8603, Japan

(Received 3 February 1997 and in revised form 19 November 1997)

A class of exact solutions of the Navier–Stokes equations is derived. Each of them represents the velocity field $\boldsymbol{v} = \boldsymbol{U} + \boldsymbol{u}$ of a thin vortical layer (a planar jet) under a uniform strain velocity field $\boldsymbol{U}$ in three-dimensional infinite space, and provides a simple flow model in which nonlinear coupling between small eddies plays a key role in small-scale vortex dynamics. The small-scale structure of the velocity field is studied by numerically analysing the Fourier spectrum of $\boldsymbol{u}$. It is shown that the Fourier spectrum of $\boldsymbol{u}$ falls off exponentially with wavenumber k for large k. The Taylor expansion in powers of the coordinate (say y) in the direction perpendicular to the vortical layer suggests that the solution may be well approximated by a function with certain poles in the complex y-plane. The Fourier spectrum based on the singularities is in good agreement with that obtained numerically, where the exponential decay rate is given by the distance of the poles from the real axis of y.

1. Introduction

In various flows, the vorticity is often confined to thin vortical layers. In order to get some insight into the fine-scale structure of such layers, let us consider the velocity field of an incompressible fluid of unit density under a uniform strain represented by

$$\boldsymbol{v}(x, y, z, t) = (ax, by, cz) + \boldsymbol{u}(x, y, t), \tag{1.1}$$

where a, b and c are constants satisfying $a + b + c = 0$ and the z-component of $\boldsymbol{u}$ is zero, i.e. $\boldsymbol{u} = (u, v, 0)$, so that the vorticity is given by $\boldsymbol{\omega} \equiv \mathrm{rot}\boldsymbol{v} = (0, 0, \omega(x, y, t))$. In terms of the stream function ψ and the vorticity $\omega = -\Delta\psi$, the Navier–Stokes equations may be casted into the form

$$\frac{\partial}{\partial t}\omega + ax\frac{\partial}{\partial x}\omega + by\frac{\partial}{\partial y}\omega + \frac{\partial(\omega, \psi)}{\partial(x, y)} = c\omega + \nu\Delta\omega, \tag{1.2}$$

$$u = \frac{\partial\psi}{\partial y},\ v = -\frac{\partial\psi}{\partial x}. \tag{1.3}$$

It is not difficult to derive exact steady solutions of (1.2) for $a = b < 0$ or $a < 0, b = 0$ (or $a = 0, b < 0$)(see e.g. Saffman 1992). The axisymmetric solution for $a = b < 0$ is sometimes referred as Burgers vortex tube, and the one-dimensional one, i.e. $\omega = \omega(x)$ ($\omega = \omega(y)$) for $a < 0, b = 0$ ($a = 0, b < 0$), as Burgers vortex layer. Turbulence models

† Present address: Department of Computational Science and Engineering, School of Engineering, Nagoya University, Chikusa-ku, Nagoya 464-8603, Japan.

which make use of random collections of such Burgers vortices give the energy spectrum

$$E(k) \propto \exp(-\beta k^2), \tag{1.4}$$

in the far dissipation range satisfying $k/k_d \gg 1$, where β is a constant and k_d is the Kolmogorov wavenumber (Townsend 1951; see the discussion in Batchelor 1953, § 7.4; and Saffman 1968). The strained-spiral vortex model of turbulence proposed by Lundgren (1982), which is consistent with the Kolmogorov energy spectrum in the inertial subrange, also yields a similar spectrum in the far dissipation range. His model makes use of approximate solutions of (1.2) in an axisymmetric external strain field, and it was shown by Pullin & Saffman (1993) that the local structure of the approximate solutions may be interpreted as that of Burgers vortex layer solution.

It is tempting to regard the uniform strain field and the field $\boldsymbol{u}$ in (1.2) as the local representations of large and small eddies, respectively. One may then interpret the terms including a, b or c in (1.2) as the interactions between the large and small eddies, and the nonlinear Jacobian term $J \equiv \partial(\omega, \psi)/\partial(x, y)$ as the nonlinear self-interaction between small eddies. The above Burgers vorticities represent solutions for which the nonlinear self-interaction vanishes identically. If the nonlinearity in $\boldsymbol{u}$, i.e. the interaction between small eddies, is neglected, the above two-dimensional model (1.2) can be generalized to include the full three-dimensionality, and the resulting three-dimensional random shear model of turbulence that neglects the nonlinearity again leads to an energy spectrum similar to (1.4) for large k/k_d (Novikov 1961; see Monin & Yaglom 1975, § 22.3).

However, recent direct numerical simulations (Kida & Murakami 1987; Kerr 1990; Chen *et al.* 1993, etc.) show that the far dissipation range spectrum falls off with the wavenumber k like $k^m \exp(-\alpha k)$ with m and α being constants. Such an exponential fall-off is also derived by a class of two-point closure or spectrum theories (Kraichnan 1959; Tatsumi 1980; Kaneda 1993). These theories suggest that interactions between small eddies of similar sizes, i.e. interactions that are local in the wavenumber space, are more important than those between eddies of very different sizes, in the dynamics governing the energy spectrum in the far dissipation range.

The difference between the two spectra, i.e. (1.4) and $k^m \exp(-\alpha k)$, suggests that some key feature of small-scale vortex dynamics may be missing in the above turbulence models. It is natural to expect that the nonlinear self-interaction between small eddies is generally non-zero in real turbulence, and the nonlinearity may play a key role in small-scale vortex dynamics. In this context, it may be worthwhile to note that Robinson & Saffman (1984) have obtained perturbatively the solutions of (1.2) for small but non-zero $\epsilon \equiv (a-b)/(a+b)$ and Reynolds number $Re = \iint \omega \mathrm{d}x\mathrm{d}y/(2\pi\nu)$. Their solutions represent non-symmetric Burgers-type vortex tubes with nonlinear interaction between small eddies. However, each term in the perturbative expansion of the solution gives an energy spectrum similar to (1.4), and it seems difficult to derive the exact analytical property of fine-scale structure from the perturbative approximate solutions, in particular for moderate or large Re. Recently, Moffatt, Kida & Ohkitani (1994) have obtained asymptotic solutions of (1.2) for large Re and for all values of ϵ. However, again it seems difficult to explain the difference of the above two spectra by using their asymptotic solution.

The study of the present paper has been motivated by these considerations. Its primary purpose is to investigate some exact solutions of (1.2) for which $J \neq 0$ and to study the fine-scale structure of the vortical layers represented by the solutions. We consider a vortical layer that is thin in one direction, say the direction of the y-axis,

in an infinite space. In § 2, we reduce (1.2) to a one-dimensional ordinary differential equation, which is nonlinear and can be characterized by the ratio $\hat{c} = c/|b|$. In § 3, it is shown numerically that for each value of $\hat{c}$, there exist a solution which represents a well-localized vortical layer (a thin planar jet). Here we use the term 'well-localized' to express the solutions whose vorticities decay as fast as exponentially for $|y| \gg 1$. The Fourier spectra of the solutions are shown in § 4 to fall off exponentially with the wavenumber k for large k, in contrast to (1.4). Regarding exponential spectra, the relationship between singularities off the real time axis and exponential frequency spectra in model equations has been identified by Frisch & Morf (1981). The analysis in § 5 clarifies the relation between singularities off the real y-axis and exponential wavenumber spectra of the steady solution of the Navier–Stokes equation. The evolution of a perturbation to the steady planar jet solution and a nonlinear coupling between a vortex layer and a planar jet are solved numerically in § 6. It is suggested that the stability depends on the imposed strain rates through the ratio $\hat{c}$, and shown that the spectrum of the time-dependent nonlinearly coupled vortex layer falls off exponentially with respect to the wavenumber k for large k, while that of uncoupled vortex layer falls off like Gaussian for large k. Section 7 is devoted to the conclusions and discussion.

2. Reduced equations representing thin vortical layers

We consider here a thin vortical layer represented by (1.1). We assume that the layer is being kept thin in the y-direction under the balance between the diffusion of vorticity and the convection of the vortex lines towards the $y = 0$ plane as well as the stretching in the z-direction by the imposed strain; this convection and stretching imply $b < 0$ and $c > 0$ in (1.2), respectively. Note that in this case, the rate of strain in the third (x)-direction is compressive for $c/|b|(\equiv \hat{c}) > 1$, while it is stretching for $\hat{c} < 1$. (Figure 1)

In terms of the non-dimensional variables defined by

$$x = (\nu/|b|)^{1/2}\hat{x}, \quad y = (\nu/|b|)^{1/2}\hat{y}, \quad t = (1/|b|)\hat{t},$$
$$\psi(x, y, t) = \nu\hat{\psi}(\hat{x}, \hat{y}, \hat{t}) \quad \text{and} \quad \omega(x, y, t) = |b|\hat{\omega}(\hat{x}, \hat{y}, \hat{t}),$$

(1.2) may be written in the following non-dimensional form:

$$\frac{\partial}{\partial\hat{t}}\hat{\omega} + (1 - \hat{c})\hat{x}\frac{\partial}{\partial\hat{x}}\hat{\omega} - \hat{y}\frac{\partial}{\partial\hat{y}}\hat{\omega} + \frac{\partial(\hat{\omega}, \hat{\psi})}{\partial(\hat{x}, \hat{y})} = \hat{c}\hat{\omega} + \hat{\Delta}\hat{\omega}, \tag{2.1}$$

where $\hat{\Delta} = (\partial/\partial\hat{x})^2 + (\partial/\partial\hat{y})^2$ and we have used $b < 0$ and $\hat{a} + \hat{c} \equiv a/|b| + c/|b| = -b/|b| = 1$. We shall omit the hats in the following for the ease of writing.

If the characteristic length scale in the x-direction is much larger than that in the y-direction, then it is tempting to expand the stream function in powers of x as

$$\psi(x, y, t) = g(y, t) + xf(y, t) + \cdots, \tag{2.2}$$

which gives

$$\omega(x, y, t) = -g''(y, t) - xf''(y, t) + \cdots.$$

Here the prime denotes the differentiation with respect to y.

The boundary conditions for g and f are to be set by taking into account the flow condition at the outer edge of the vortical layer. We require here that the flow tends

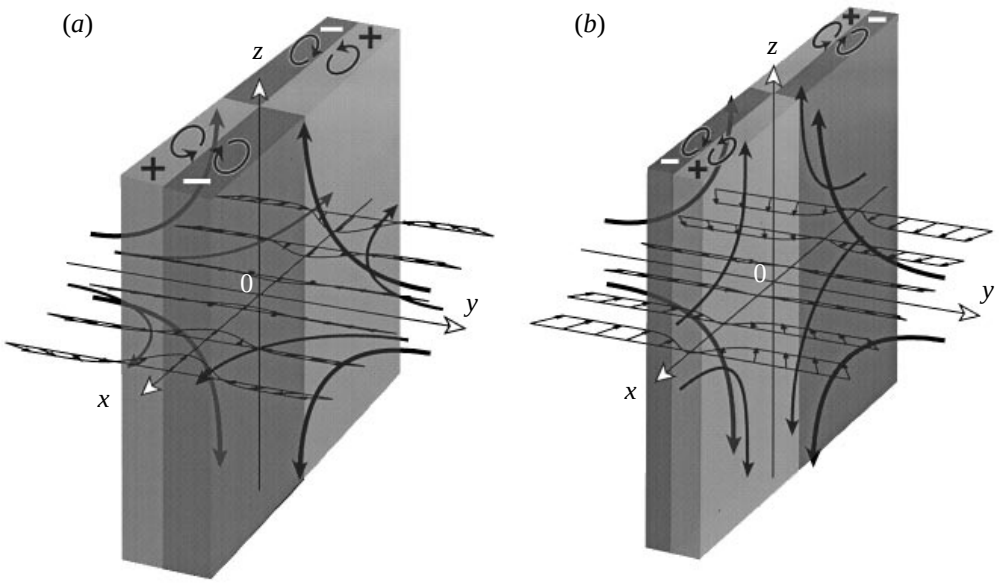

FIGURE 1. Sketch of the strain field (*a*) $\hat{c} < 1$ and (*b*) $\hat{c} > 1$. The direction of the strain flow is indicated on its streamline. The vortical layer obtained in § 3 forms a vortex quadrapole as illustrated (*a*) for $\hat{c} < 1.5$ and (*b*) $\hat{c} > 1.5$, where vorticities are parallel to the z-axes and in the positive z-direction in the light grey region and negative in the dark grey region. Typical velocity profiles, (*a*) for $c \approx 0.8$ and (*b*) for $c \approx 3.0$, in the (x, y)-plane are also illustrated, showing, respectively, the inward and the outward planar jets superposed on background strain field.

to $((1-c)x, -y, cz)$ (i.e. (ax, by, cz) in the dimensional form) at the outer edge of the layer, i.e.

$$|g'(y,t)| \to O(|y|^0), \tag{2.3}$$

and

$$|f(y,t)| \to o(|y|^1), \ |f'(y,t)| \to 0, \tag{2.4}$$

as $|y| \to \infty$, which respectively imply

$$|u| = |(\partial\psi/\partial y)| = |g' + xf'| \to O(|y|^0),$$

and

$$|v| = |-(\partial\psi/\partial x)| = |-f| \to o(|y|^1),$$

as $|y| \to \infty$ with $|x|$ being finite. Note that condition (2.4) admits not only solutions for which $|v| = O(|y|^0)$ for large $|y|$ but also solutions for which $|v|$ is smaller in amplitude than the linear imposed strain but unbounded for large $|y|$. It is possible to exclude such unbounded or non-localized solutions by imposing exponential decay of $|f'|$ as $|y| \to \infty$, instead of (2.4). In fact, it will be shown in § 3 that such a well-localized solution may be found for each value of $c\,(>0)$.

A class of exact solutions of (2.1) satisfying the above boundary conditions can be obtained by retaining only the g- and f-terms and discarding the other terms in (2.2). In fact, it is shown that (2.1) is satisfied by (2.2) with only the g- and f-terms retained, provided that

$$\frac{\partial}{\partial t}(-g'') + yg''' + cg'' + g^{\mathrm{iv}} = f''g' - g'''f, \tag{2.5}$$

and

$$\frac{\partial}{\partial t}(-f'') + (1 - 2c + f')(-f'') - (y + f)(-f''') + f^{\mathrm{iv}} = 0. \tag{2.6}$$

The simplest class of exact solutions in the context of using the expansion (2.2) is obtained by substituting $f = 0$, which is a solution of (2.6), into (2.5). For a steady state, it gives

$$(yg'')' + (c - 1)g'' + g^{\mathrm{iv}} = 0. \tag{2.7}$$

This equation can be solved analytically, and the solution may be in general expressed in terms of confluent hypergeometric functions. For $c = 1$, the solution is particularly simple, and under the boundary condition (2.3) it represents the Burgers vortex layer:

$$\omega \equiv -g'' = \omega_0 \exp\left(-\tfrac{1}{2}y^2\right),$$

where ω_0 is an arbitrary constant. This solution incorporates three fundamental features of vortex dynamics, i.e. stretching, convection and viscous diffusion of vorticity. However, (2.7) is linear in g, and its solution cannot represent the nonlinear self-interaction between the small eddies. It is also shown from (2.7) that the spectrum defined by

$$\omega(y) = \int_{-\infty}^{\infty} \hat{\omega}(k)\, \mathrm{e}^{\mathrm{i}ky}\, \mathrm{d}y$$

falls off like

$$\hat{\omega}(k) \propto |k|^{c-1} \mathrm{e}^{-k^2/2},$$

at high $|k|$. Thus the solution of (2.7) cannot explain the exponential fall off of the energy spectrum at high $|k|$, and it is necessary to keep the f-term in (2.2) for deriving solutions that can represent the nonlinear self-interaction between small eddies.

A simple class of exact solutions that represent the nonlinear interaction may be derived by retaining only the f-term instead of g-term in (2.2), i.e. by putting

$$\psi(y, t) = xf(y, t), \tag{2.8}$$

which gives

$$u = xf'(y, t), \quad v = -f(y, t) \quad \text{and} \quad \omega = -xf''(y).$$

Equation (2.6) is independent of g, and in the following we analyse the solution of (2.6) subject to the boundary condition (2.4). The solutions obtained by retaining the g-term as well as f-term will be discussed in § 6.

In terms of F defined by $F(y, t) = -y - f(y, t)$, (2.6) and (2.4) may be written as

$$\frac{\partial}{\partial t}F'' - 2cF'' - F^{\mathrm{iv}} - F'F'' + FF''' = 0, \tag{2.9}$$

and

$$F(y, t) \to -y, \quad F'(y, t) \to -1 \quad \text{as} \quad y \to \pm\infty. \tag{2.10}$$

Integrating (2.9) once with respect to y gives

$$\frac{\partial}{\partial t}F' - 2cF' - F''' - (F')^2 + FF'' = 2c - 1, \tag{2.11}$$

where the integration constant has been determined by the boundary condition at $y \to \pm\infty$. The steady exact solutions $F(y)$ may be therefore obtained from

$$-2cF' - F''' - (F')^2 + FF'' = 2c - 1, \tag{2.12}$$

and (2.10).

c	$F'(0)$	c	$F'(0)$	c	$F'(0)$
0.2	0.777 027 354 82	1.2	−0.577 253 1	2.2	−1.995 780
0.4	0.521 390 881	1.4	−0.858 733 5	2.4	−2.281 927
0.6	0.253 534 375	1.6	−1.141 565	2.6	−2.568 62
0.8	−0.020 222 47	1.8	−1.425 472	2.8	−2.855 78
1.0	−0.297 532 6	2.0	−1.710 259	3.0	−3.143 35

TABLE 1. Values of $F'(0)$ satisfying the criterion $|F'(20.0) - (-1)| < 10^{-7}$.

It may be worthwhile to note that when $c = 0$, (2.12) is reduced to the equation first derived by Falkner & Skan (1931) in the study of boundary layer equations. The equation with $c = 0$ is also known to represent steady two-dimensional flow towards a stagnation point on a rigid boundary placed at $y = 0$ (see e.g. Batchelor 1967).

3. Steady solution representing a planar jet in a strain field

The solution of (2.12) satisfying the boundary condition (2.10) may be obtained numerically by using a shooting method regarding $F(0)$, $F'(0)$ and $F''(0)$ as adjustable parameters; they are to be adjusted in such a way that F satisfies $F(y) \to -y$ as $|y| \to \infty$. In this section, we confine ourselves to the antisymmetric, i.e. odd, solutions satisfying $F(-y) = -F(y)$, for the sake of simplicity. It is readily shown that the antisymmetry is compatible with (2.12). Since $F(0) = F''(0) = 0$ for any odd function F, the only remaining parameter to be determined is $F'(0)$. For the numerical integration of (2.12), we used a fourth-order Runge–Kutta method with $\Delta y = 0.001$, and in practice, we used the criterion that the boundary condition (2.10) may be regarded to be satisfied if $|F'(20.0) - (-1)| < \epsilon \ll 1$. In table 1, the values of $F'(0)$ thus obtained for $\epsilon = 10^{-7}$ are listed for each value of c. (The reason why the number of significant figures is not the same in the table will be given at the end of this section.) Our experience in the numerical computation suggests (i) the value of $F'(0)$ for which the above criterion is met depends on c almost linearly (as will be seen in figure 8), (ii) for a fixed c, the dependence of $F'(20.0)$ on $F'(0)$ also looks almost linear, when the value of $F'(0)$ is close to the one listed in table 1. We can therefore obtain the values of $F'(0)$ in table 1 in a systematic way. Further detailed computations suggest that this is also the case for values of ϵ less than 10^{-7}.

Since (1.1), (1.3) and (2.8) give

$$\boldsymbol{u}(x, y) = (u, v, 0) = (xf'(y), -f(y), 0) \quad \text{and} \quad \omega(x, y) = -xf''(y),$$

the plots of the numerical solutions, (*a*) $-f(y)$, (*b*) $f'(y)$ and (*c*) $-f''(y)$, in figure 2 give the profiles of (*a*) v, (*b*) u/x and (*c*) ω/x as functions of y, respectively. Remember that $f(y)$ is assumed to be an odd function of y so that f' and f'' are even and odd functions, respectively. The vorticity $\omega(x, y)$ under consideration therefore has the following symmetry:

$$\omega(x, y) = -\omega(-x, y) = -\omega(x, -y).$$

The solution, therefore, represents a vortex quadrapole in the linear imposed strain. As shown in figure 2(*b*), the flow field is an outward planar jet for $c > 1.5$ and an inward jet for $c < 1.5$ superposed on the linear strain field for each c (see also figure 1).

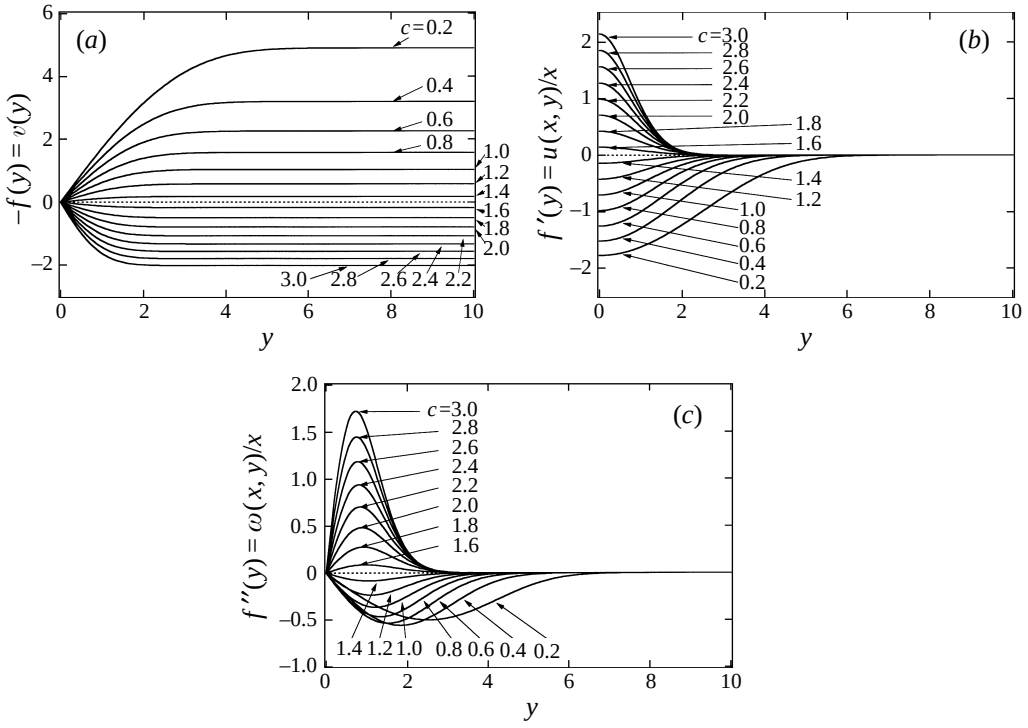

FIGURE 2. Profiles of the steady solutions for $c = 0.2, 0.4, \cdots, 3.0$: (*a*) $-f(y) = v(y)$, (*b*) $f'(y) = u(x, y)/x$ and (*c*) $-f''(y) = \omega(x, y)/x$.

Figure 2(*b*) and 2(*c*) suggest that the vorticities are well-localized and that u and ω have finite supports in y outside which they are negligibly small. In order to see this point more clearly and to clarify the relation between the boundary condition (2.10) and the criterion with the different values of $\epsilon\,(\ll 1)$, we study the asymptotic nature of the exact solutions for $|y| \to \infty$ in some detail below.

Asymptotic behaviour of the solution for large $|y|$

According to the boundary condition (2.4), the asymptotic behaviour of the solution of (2.6) for large y at steady state is determined by the following linear equation:

$$f''' + yf'' - (2 - 2c)f' = 0. \tag{3.1}$$

It is readily shown that $f' = A\mathrm{e}^{-y^2/4}\mu(y)$ satisfies (3.1) provided that

$$\mu'' + (\lambda + \tfrac{1}{2} - \tfrac{1}{4}y^2)\mu = 0, \tag{3.2}$$

where A is a constant and $\lambda = 2c - 3$. The solution of (3.2) can be in general written by a linear combination of $D_\lambda(y)$ and $D_{-\lambda-1}(\mathrm{i}y)$, where $D_\lambda(y)$ is the so-called parabolic cylinder function (see, for example, Magnus & Oberhettinger 1954). By using the asymptotic expressions for $D_\lambda(y)$ and $D_{-\lambda-1}(\mathrm{i}y)$ for large y, we have

$$f'(y) \sim A_1\mathrm{e}^{-y^2/2}y^{2c-3} + A_2y^{2-2c} \quad \text{as} \quad y \to \infty, \tag{3.3}$$

where A_1 and A_2 are constants which may depend on e.g. the values of $f'(0)$ and $f''(0)$

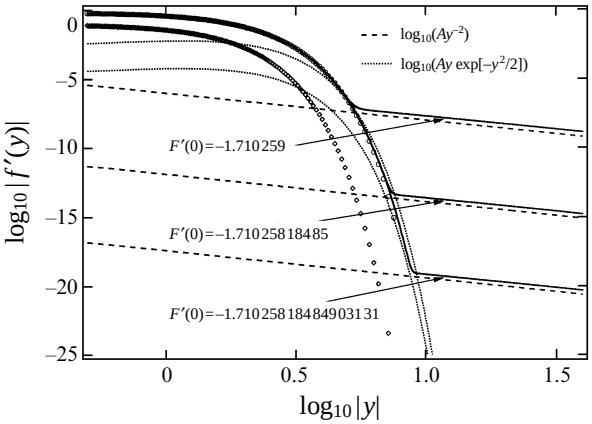

FIGURE 3. Plots of $\log_{10}|f'(y)|$ vs. $\log_{10}|y|$ by the numerical solutions for $c = 2.0$ with slightly different values of $F'(0)$ as indicated in the figure (solid lines). Broken lines indicate asymptotic forms (3.3) with $A_2 = 0$ and $A_2 \neq 0$. Time-dependent solutions of (2.6) subject to (6.2) with $\epsilon = 0.1$ are also plotted for a comparison; $t = 0$ ($\diamond$) and $t = 12.0$ ($\circ$).

of the steady solution of (2.6). (For large $-y$, $f'(y) \sim A_1 e^{-y^2/2}|y|^{2c-3} + A_2|y|^{2-2c}$, since $f'(-y) = f'(y)$.) When $A_2 \neq 0$, the second term in (3.3) dominates the behaviour of f' for large y, so that $f' \propto y^{2-2c}$ for large y and (2.4) is not satisfied for $c < 1$. The algebraic growth of $|f'|$ for large y contradicts (2.10). On the other hand, however, when $A_2 = 0$, not only (2.4) but also the boundary condition which requires f' to decay exponentially as $|y| \to \infty$, can be satisfied irrespectively of c (provided that such a solution exists). The solution for which $A_2 = 0$ and $f'(-y) = f'(y)$ represents a well-localized planar jet or a vortex quadrapole well-localized in a layer.

In order to find the well-localized solution, we perform numerical computations in the following by using a fourth-order Runge–Kutta algorithm with $\Delta y = 0.000\,01$ in 31-digits arithmetic. (As a check to confirm that the results are not affected by the particular choice of the solution method, we also used a Bulirsch–Stoer method (in Press *et al.* 1988) for the integration; there was no significant difference between the results by the two solution methods.)

Figure 3 shows the dependence of the numerical solutions for $c = 2$ on the value of $F'(0)$, where we have used the values of $F'(0)$ such that (i) the criteria $|F'(20) - (-1)| < \epsilon$ with $\epsilon = 10^{-7}$, 10^{-12} and 10^{-17} are respectively satisfied, (ii) the resulting $f'(y)$ are everywhere positive as shown in figure 2(*b*), and (iii) if each of the last numbers of the significant digits of the $F'(0)$ is increased by 1 (e.g. when $-1.710\,258$ is used instead of $-1.710\,259$), then $f'(y)$ changes its sign as y increases. By utilizing these properties, we can add significant digits to $F'(0)$ systematically. It can be observed in figure 3 that each f' with slightly different $F'(0)$ behaves like a Gaussian for small y and behaves like $|f'| \sim Ay^{\mu}$ for large y, where A is a constant depending on $F'(0)$ and $\mu \approx 2 - 2c$ ($= -2.0$ for $c = 2.0$), in good agreement with (3.3) with $A_2 \neq 0$. It is observed in the figure that the value of $A\,(> 0)$ is of order ϵ used in (i) mentioned above, and also that A is smaller and the range of y where f' behaves like a Gaussian is wider for $F'(0)$ with more significant digits. Note that the solutions show a good agreement with each other for small $|y|$ where each f' behaves like a Gaussian and also that in that region the asymptotic form of f' for large y is well approximated by

$A_1 e^{-y^2/2} y^{2-2c}$ which is obtained by putting $A_2 = 0$ in (3.3). Similar computations for different values of $c \in (0, 3.0)$ yielded results qualitatively similar to those for $c = 2.0$.

The results show that the behaviour of the numerical solutions for large y is consistent with (3.3). They also suggest that by determining the value of $F'(0)$ precisely, we can find for each c a unique (at least locally in the $F'(0)$-space) solution which behaves like (3.3) with $A_2 = 0$ for large y. Recently an equation similar to (2.12) has been studied in detail by Phillips (1996) in the context of unsteady boundary layers, and it has been shown that to ensure uniqueness, not only must exponential decay be imposed but also whether the flow may or may not reverse must be specified (see also discussion in Brown & Stewartson 1965 and Buckmaster 1973). For the present problem, as suggested by the process of reducing A_2, the solution with $F(0) = F''(0) = 0$ seems to be uniquely determined, if we impose exponential decay as boundary condition instead of (2.10) upon the solution of (2.12) for $c > 1$. In the following section, we shall mainly focus on the solution with well-localized vorticity, obtained by using the specific value of $F'(0)$ for each $c \in (0, 3)$, and in practice we shall regard the numerical solutions obtained by using e.g. $F'(0)$ listed in table 1 as approximations for such 'well-localized' solutions.

4. Fourier spectrum of the steady velocity field

In this section, we study the fine scale structure of $\boldsymbol{u} = (u, v, 0)$ by analysing its Fourier spectrum. In terms of f or F, we have

$$u = \frac{\partial \psi}{\partial y} = x f'(y) = x(-1 - F'(y)), \tag{4.1}$$

$$v = -\frac{\partial \psi}{\partial x} = -f(y) = y + F(y), \tag{4.2}$$

where $F(y) \sim -y$ for large $|y|$. Since $u(x, y)/x$ does not depend on x, in the rest of this paper we regard $u(x, y)/x$ as $u(y)$.

Let us consider the Fourier transform of $u(y) = f'(y) = -1 - F'(y)$ defined by

$$\hat{u}(k) = \int_{-\infty}^{\infty} u(y)\, e^{-iky} dy, \tag{4.3}$$

and write $\hat{u}$ as

$$\hat{u}(k) = \int_{-Y}^{Y} u(y)\, e^{-iky} dy + R(Y, k). \tag{4.4}$$

Then the first term on the right-hand side of (4.4) may give a good approximation to $\hat{u}(k)$, provided that $|u(y)|$ is negligibly small for $|y| > Y$ and therefore the residual $R \ll 1$ for sufficiently large Y. Partial integrations show that $|R(Y, k)| = O(|u'(Y)|/k^2)$ for large k and Y, where we have used $u(-y) = u(y)$. Therefore, the above approximation is useful if $|u'(Y)| \ll 1$ and $|u(y)|$ is negligibly small for $|y| > Y$. (As shown in § 3, we can reduce $|R(Y, k)|$ as small as we like within the computational accuracy by determining the value of $F'(0)$ precisely.)

Let $\bar{u}$ be defined by $\bar{u}(y) = u(y)$ for $|y| \leqslant Y$ and 0 for $|y| > Y$. Then the following

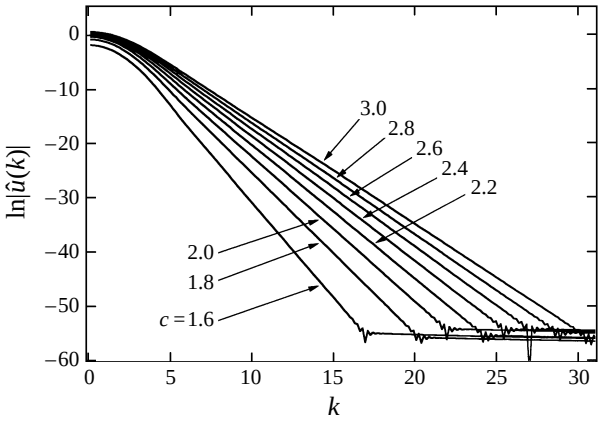

FIGURE 4. Plots of $\ln|\hat{u}(k)|$ vs. k obtained by using fast Fourier transform of the steady solutions $u(y) = f'(y)$ for $c = 1.6, 1.8, \cdots, 3.0$.

$2Y$-periodic function can be expanded in a Fourier series:

$$\sum_{j=-\infty}^{\infty} \bar{u}(y + 2jY) = \sum_{p=-\infty}^{\infty} c_p \exp(\mathrm{i}\pi py/Y), \tag{4.5}$$

where

$$c_p = \frac{1}{2Y} \int_{-Y}^{Y} u(y)\, \mathrm{e}^{-\mathrm{i}\pi py/Y}\, \mathrm{d}y, \tag{4.6}$$

which gives a discrete approximate sampling of $\hat{u}(k)$ as $\hat{u}(\pi p/Y) = 2Yc_p$ ($p = 0, \pm 1, \cdots$). For the evaluation of c_p, we use a discrete fast Fourier transform of the data for $-Y < y < Y$ which satisfies the criterion $|u(Y = 20.0)| < 10^{-17}$ for each value of c.

We have two types of spectrum $\hat{u}(k)$: one is obtained for $0 < c < 1.5$ and the other for $c > 1.5$. The latter type is rather simpler in behaviour than the former and as will be seen in § 6 the range of c of most interest in this paper is $c > 1.5$. We therefore begin with the numerical analysis of the latter spectrum.

Spectrum $\hat{u}(k)$ for $c > 1.5$

It can be observed in figure 4 that for large k, say $4 < k\,(< K)$, the spectrum falls off exponentially with respect to k. Here K depends on c; e.g. $K \approx 21$ for $c = 2.0$. As shown in § 3, the numerical solutions for $c > 1$ behave like $u(y) \sim Ay^{\mu}$ for large y, where $\mu = 2 - 2c$ and A is a constant whose magnitude is restricted by the criterion specifying the magnitude of u at $y = 20$, so that R in (4.4) is evaluated to be $R(Y, k) \approx A(2 - 2c)Y^{1-2c}/k^2$ for large k, which may explain the behaviour of the values of $\ln|\hat{u}(k)|$ for $k > K$ in figure 4.

If we assume that $|\hat{u}(k)| = k^{\gamma}\mathrm{e}^{-\alpha k+\beta}$, α, β and γ can be determined (as functions of k) by solving a system of linear equations, $\ln|\hat{u}(k)| = -\alpha k + \beta + \gamma \ln k$, with $(Y/\pi)k = p - 1, p, p + 1$ for each $p = 2, 3, \cdots$. Figure 5(a) suggests that the value of α for each c tends asymptotically to a certain constant as k becomes large. The values of α as well as its asymptotic values are smaller for larger c. This fact implies that the small scales are more excited for large c. Note that c is the normalized strain rate in the direction of the vorticity. The asymptotic value of α will be shown in the next section to be closely related to the smallest distance of the singularities of the

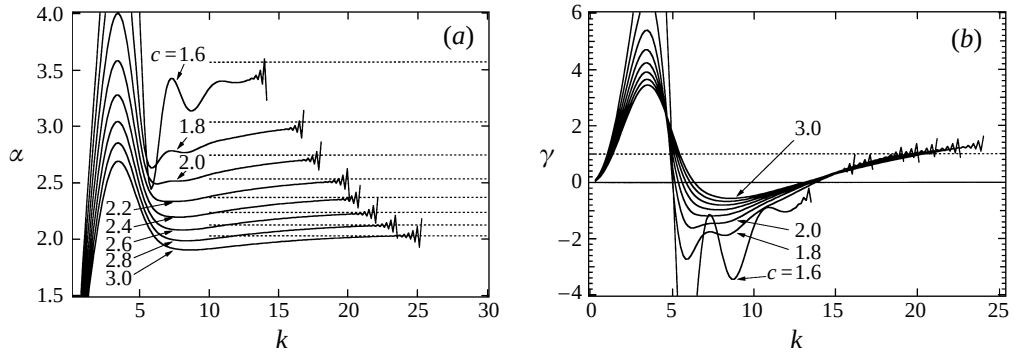

FIGURE 5. Plots of the values of (*a*) α and (*b*) γ obtained (as functions of k) by assuming that the data plotted in figure 4 have the k-dependence $|\hat{u}(k)| = k^{\gamma}\mathrm{e}^{-\alpha k+\beta}$. The broken lines in (*a*) show the values of $\mathrm{e}^{p/2}$ listed in table 2; $c = 1.6, 1.8, \cdots, 3.0$ from the top to the bottom.

solution from the real y-axes in the complex y-plane. Figure 5(*b*) suggests that the dependence of γ on c becomes weak for large k and that the value of γ tends to a constant asymptotically.

Spectrum $\hat{u}(k)$ *for* $0 < c < 1.5$

It is seen in figure 6 that the spectrum decays exponentially with an oscillation with respect to k for large $k\,(< K)$. (It can be observed that value of K for $c = 1.0$ is especially larger than those for the other values of c. The reason may be because the truncation error $R(Y,k)$ is exactly zero for $c = 1$; the values of $f'(y)$ for $c = 1.0$ are observed to settle down to a constant for large y, showing a good agreement with the result of the simple analysis for asymptotic behaviour of the solution for large y in § 3, i.e. algebraic decay rate $\mu = 2 - 2c = 0$ for $c = 1$.) Note that exponential decay rates of the spectra for $c \in (0, 1.5)$ show no significant dependence on c. Note also that the spacings between the successive minima are almost the same in each of the wavy curves and that they are larger for larger c within the range $(0, 1.5)$. The behaviour of the above wavy spectra for $c \in (0, 1.5)$ as well as that for $c \in (1.5, 3.0)$ will be interpreted well in the next section in terms of the singularities of the solution.

5. Singularities in the complex y-plane

In the previous section, it has been shown that solutions of (1.2) have small-scale structure characterized by the exponential fall-off of the Fourier spectrum with wavenumber k for large k. We investigate in this section the analytic structure of the solution of (2.12) in the complex y-plane. For that purpose, we analyse the Taylor series expansions at $y = 0$ of the solutions, and study the nature of the singularities which are the nearest to $y = 0$ in the complex y-plane. We then discuss the relation between the singularities and the Fourier spectrum.

Let the solution of (2.12) be expressed in a Taylor series expansion:

$$F(y) = \sum_{n=0}^{\infty} a_n y^n. \tag{5.1}$$

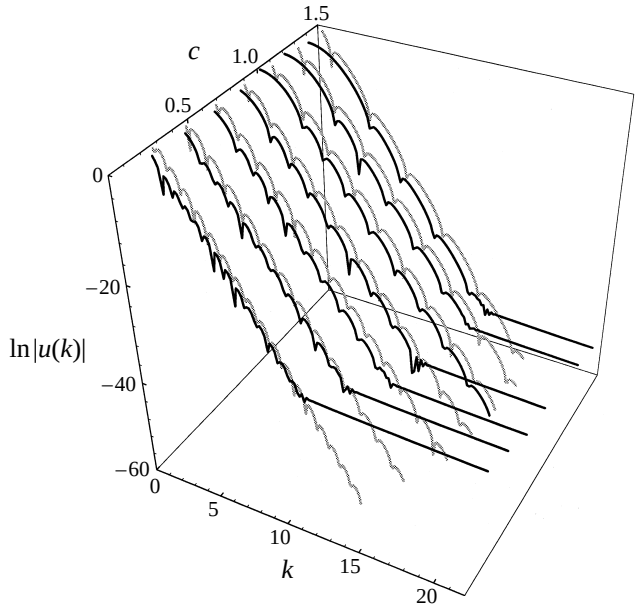

FIGURE 6. Plots of $\ln|\hat{u}(k)|$ vs. k obtained by using fast Fourier transform of the steady solutions $u(y) = f'(y)$ for $c = 0.2, 0.4, \cdots, 1.4$ (black lines). The spectra given by (5.9) are also plotted (grey lines).

Then substitution into (2.12) leads to the following relation among the Taylor coefficients:

$$n(n-1)(n-2)a_n = -2c(n-2)a_{n-2} + \sum_{j=0}^{n-3}(j+2)(j+1)a_{n-j-3}a_{j+2} - \sum_{j=0}^{n-3}(n-j-2)(j+1)a_{n-j-2}a_{j+1}. \quad (5.2)$$

The coefficients a_n for $n \geqslant 3$ may be determined recursively by (5.2) from any given a_0, a_1 and a_2. Since the solutions discussed in §3 are odd functions in y, we put here $a_0 = a_2 = 0$ and $a_1 = F'(0)$, where we use the value of $F'(0)$ listed in table 1 for each c.

Figure 7 shows the comparison of $F'(y)$ obtained in § 3 for $c = 2$ with that of

$$F'(y)^{(N)} = \frac{\mathrm{d}}{\mathrm{d}y}\left(\sum_{n=0}^{N} a_n y^n\right),$$

with $N = 50, 100, 150$ or 200, where a_n are numerical solutions of (5.2) with $c = 2$ and $a_0 = a_2 = 0$, $a_1 = -1.710\,259$. It can be observed that the numerical solutions agree well for $|y| < A^{(N)}$, in spite of the difference of the solution method, where $A^{(N)}$ is the value of y at which $|F'(y)^{(N)}|$ shows a rapid growth. The N-dependence of $A^{(N)}$ observed in figure 7 suggest that there exists a limit $A^{(\infty)}$. This implies that $A^{(\infty)}$, which depends on c, gives the radius of convergence of Taylor series expansion (5.1) and there exist singularities on the circle defined by $|y| = A^{(\infty)}$ in the complex y-plane.

The singularities, which are expected to be on the circle of convergence, may

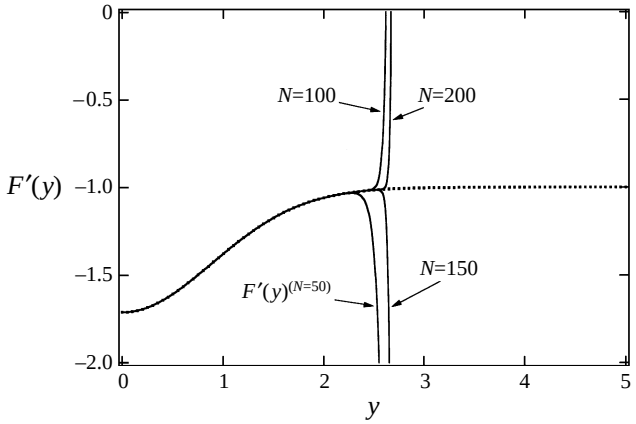

FIGURE 7. Plots of $F'(y)$ of the numerical solution for $c = 2.0$ obtained in § 3 (dotted curve) and $F'(y)^{(N)}$ with $N = 50, 100, 150$ or 200 (solid curves).

be characterized by numerically analysing the dependence of a_n on n. The analysis suggests that for large j,

(i) $|a_{2j-1}| \sim \mathrm{e}^{-pj+q}$, irrespectively of c, where p and q may be estimated by using a least-square fitting to the data $\ln|a_{2j-1}|$,

(ii) $(-1)^j a_{2j-1}/\mathrm{e}^{-pj+q} \sim 1$ for $c > 1.5$ and $(-1)^j a_{2j-1}/\mathrm{e}^{-pj+q} \approx C\cos(2\Theta j)$ for $0 < c < 1.5$ with C and Θ being constants.

(As readily shown inductively from (5.2), a_{2j} for $j > 1$ are all zeros if $a_0 = a_2 = 0$, which confirms that F is an odd function of y when $F(0) = F''(0) = 0$.) It may be interesting to note that the remarkable change of the behaviour of the Taylor coefficients as well as that of Fourier spectrum observed in the previous section occurs at $c = 1.5$.

Since

$$\sum_{j=1}^{\infty}(-1)^j \mathrm{e}^{-pj+q} y^{2j-1} = \mathrm{e}^q y^{-1} \sum_{j=1}^{\infty}\left(-\frac{y^2}{\mathrm{e}^p}\right)^j = -\tfrac{1}{2}\mathrm{e}^q\left(\frac{1}{y - \mathrm{i}\mathrm{e}^{p/2}} + \frac{1}{y + \mathrm{i}\mathrm{e}^{p/2}}\right), \tag{5.3}$$

and

$$\sum_{j=1}^{\infty}(-1)^j C\cos(2\Theta j)\,\mathrm{e}^{-pj+q} y^{2j-1} = \frac{C}{2}\mathrm{e}^q y^{-1}\left\{\sum_{j=1}^{\infty}\left(-\frac{y^2}{\mathrm{e}^{p-2\mathrm{i}\Theta}}\right)^j + \sum_{j=1}^{\infty}\left(-\frac{y^2}{\mathrm{e}^{p+2\mathrm{i}\Theta}}\right)^j\right\}$$
$$= -\frac{C}{4}\mathrm{e}^q\left(\frac{1}{y - \mathrm{i}\mathrm{e}^{p/2-\mathrm{i}\Theta}} + \frac{1}{y + \mathrm{i}\mathrm{e}^{p/2-\mathrm{i}\Theta}} + \frac{1}{y - \mathrm{i}\mathrm{e}^{p/2+\mathrm{i}\Theta}} + \frac{1}{y + \mathrm{i}\mathrm{e}^{p/2+\mathrm{i}\Theta}}\right), \tag{5.4}$$

the behaviour of the Taylor coefficients as mentioned above suggests that $F(y)$ has poles of order 1 at $y = \pm\mathrm{i}\mathrm{e}^{p/2}$ for $c \in (1.5, 3.0)$, and at $y = \pm\xi$, $\pm\xi^*$ for $c \in (0, 1.5)$, respectively, where $\xi \equiv \mathrm{e}^{p/2}\mathrm{e}^{\mathrm{i}(\pi/2-\Theta)}$ and asterisk denotes the complex conjugate.

These singularities, i.e. poles of order 1, are consistent with the following simple analysis based on (2.12). Let us assume that a solution of (2.12) can be expressed locally as

$$F(y) \sim B(y - y_0)^{\lambda} \tag{5.5}$$

near a singularity $y = y_0$, where $\mathrm{Re}(\lambda) < 0$ and B are constants to be determined.

c	ξ	c	$e^{p/2}i$	$e^q/2$
0.2	4.155 + 4.923 i	1.6	3.570 i	6.27
0.4	2.845 + 4.518 i	1.8	3.038 i	6.33
0.6	2.569 + 4.047 i	2.0	2.743 i	6.23
0.8	2.090 + 3.922 i	2.2	2.533 i	6.14
1.0	1.728 + 3.850 i	2.4	2.370 i	6.07
1.2	1.418 + 3.840 i	2.6	2.237 i	6.02
1.4	1.094 + 3.992 i	2.8	2.126 i	5.98
1.5	—	3.0	2.031 i	5.95

TABLE 2. Locations of singularities detected from Taylor expansions.

Substituting (5.5) into (2.12) and keeping only the dominant terms near $y = y_0$ gives $\lambda = -1$ and $B = -6$, and shows that $-F'''$ and $FF'' - F'^2$ balance each other there. The location y_0 of the singularity is to be determined by the equation and the boundary condition. Note that the balance of the terms $-F'''$ and $FF'' - F'^2$ in (2.12) can be regarded as the balance of the viscosity and the nonlinear terms in (1.2).

From (5.3) and (5.4), $e^{p/2}$ may be understood as the radius of convergence of the corresponding Taylor series. It follows that the distances (from the real y-axes) of the poles which are nearest to $y = 0$ are $e^{p/2}$ for $c > 1.5$ and $e^{p/2}\cos\Theta$ for $0 < c < 1.5$. The value of Θ may be easily estimated numerically by substituting $y = e^{p/2}e^{i\theta}$ into e.g. $|F(y)^{(200)}|$ and plotting it as a function of θ; the angle θ which gives the peak value of $|F^{(200)}|$ gives $\pi/2 - \Theta$. (We tried the other values of $N(> 200)$ to estimate Θ and found no significant changes in the results.) Table 2 lists the locations of the singularities in $0 \leqslant \theta \leqslant \pi/2$ thus evaluated for various values of c. For $c \in (1.5, 3.0)$, the values of $e^q/2$ are also listed in the table, which show a fairly good agreement with $|B| = 6$ obtained in the above simple analysis. This fact suggests that the function $F(y)$ for $c \in (1.5, 3.0)$ may be well characterized by the singularities $-6/(y \pm e^{p/2}i)$ in the complex y-plane.

Asymptotic evaluation of the Fourier spectrum (4.3) as $k \to \infty$ may be done by taking account of singularities with the smallest imaginary part (e.g. Murray 1984). Let us assume that $F(y)$ as $y \to 0$ is well approximated by (5.3) and (5.4) and that the singularities given by (5.3) and (5.4) dominate the asymptotic behaviour of the Fourier spectrum as $k \to \infty$. Then the asymptotic evaluation of the Fourier transform for $k \to \infty$ is straightforward. From (5.3) and (5.4), we have for $c > 1.5$,

$$u(y) = -1 - F'(y) = -\tfrac{1}{2}e^q \left(\frac{1}{(y - ie^{p/2})^2} + \frac{1}{(y + ie^{p/2})^2} \right) + \varphi_a(y), \tag{5.6}$$

and for $0 < c < 1.5$,

$$u(y) = -\frac{C}{4}e^q \left(\frac{1}{(y - ie^{p/2-i\Theta})^2} + \frac{1}{(y + ie^{p/2-i\Theta})^2} + \frac{1}{(y - ie^{p/2+i\Theta})^2} + \frac{1}{(y + ie^{p/2+i\Theta})^2} \right) + \varphi_b(y), \tag{5.7}$$

respectively, where $\varphi_a(y)$ and $\varphi_b(y)$ may be regarded as the terms due to non-dominant singularities. By evaluating the residue of $u(y)e^{-iky}$ at the singularities that

are in $\mathrm{Im}(y) < 0$ and given by (5.6) and (5.7), we obtain the following asymptotic spectra for $k \gg 1$:

for $c > 1.5$

$$\hat{u}(k) = \int_{-\infty}^{\infty} u(y)\mathrm{e}^{-\mathrm{i}ky}\mathrm{d}y \approx -\tfrac{1}{2}\mathrm{e}^{q}\pi k \exp(-\mathrm{e}^{p/2}k), \tag{5.8}$$

for $0 < c < 1.5$

$$\hat{u}(k) \approx -\frac{C}{2}\mathrm{e}^{q}\pi k \cos(\mathrm{Re}(\xi)k)\exp(-\mathrm{Im}(\xi)k), \tag{5.9}$$

where $\xi = \mathrm{e}^{p/2}\mathrm{e}^{\mathrm{i}(\pi/2-\Theta)}$ with $0 < \Theta < \pi/2$.

In § 4, we assumed that $\hat{u}(k) = \beta k^{\gamma}\exp(-\alpha k)$ for $c \in (1.5, 3.0)$ and estimated α and γ by using the data plotted in figure 4. Spectrum (5.8) for $c \in (1.5, 3.0)$ implies (i) α is given by $\mathrm{e}^{p/2}$, which is the distance of the dominant singularities from the real y-axes in the complex y-plane, and (ii) $\gamma \to 1$ as $k \to \infty$ irrespectively of the value of c. In figure 5(*a*), we also plot the values of $\mathrm{e}^{p/2}$ listed in table 2. It is seen from the figure that the asymptotic values of α for large k obtained in § 4 agree well with the corresponding values of $\mathrm{e}^{p/2}$. In addition, the fact that the values of γ tend to a constant (≈ 1) independent of the values of c, which was observed in figure 5(*b*), is consistent with (ii). It may be understood that (5.8) gives an asymptotic form of the spectrum $\hat{u}(k)$ for large k.

The wavy nature of the spectrum observed in figure 6 may be understood well by (5.9). According to (5.9), the exponential decay rate of the spectrum for $c \in (0, 1.5)$ is given by $\mathrm{Im}(\xi) = \mathrm{e}^{p/2}\cos\Theta$ and the spacings Δk between the minima of the wavy spectrum observed in figure 6 by $\pi/\mathrm{Re}(\xi)$. The spectrum (5.9), which is based on the Taylor series expansions, can be obtained by using the values of ξ listed in table 2, q obtained by a least-square fitting as mentioned before and $C \approx 2.0$ which is estimated from the plot of $(-1)^j a_{2j-1}/\mathrm{e}^{-pj+q}$ vs. j (omitted). The two curves for each value of c in figure 6 show a good agreement especially for large $k\,(< 18)$. For the values of c less than about 0.5, there are discrepancies between the two curves. This suggests that for these cases the singularities detected by the Taylor expansion about $y = 0$ no longer dominate the asymptotic behaviour of $\hat{u}(k)$ for large k, but the other ones which are nearer to the real y-axes dominate it. In fact, by using Taylor expansions with centre shifted from $y = 0$, we found other singularities which are nearer to the real y-axes than those listed for $c = 0.2$ and 0.4 in table 2. (The Taylor expansions about $y = y_0$ may be obtained by solving (5.2) with $a_0 = F(y_0), a_1 = F'(y_0)$ and $a_2 = F''(y_0)/2$, whose values are obtained by using the expansion about $y = 0$.)

6. Time-dependent planar jet and vortex layer solutions

The planar jet solution, whose small-scale structure is analysed in the previous sections, is derived on the basis of the assumption that the characteristic length scale in the x-direction is much larger than that in y, as implied in the expansion of the stream function as in (2.2), or the assumption $\psi(x, y, t) = g(y, t) + xf(y, t)$. In this section, on the basis of the same assumption, we study the properties of the time-dependent solutions of (2.5) and (2.6) numerically, by considering a particular kind of initial conditions. First, in order to get some idea of the stability of

the steady solutions of (2.6), we assume $g = 0$ and consider the following initial conditions:

$$f'(y,0) = f'_{(steady)}[c](y) + \epsilon \exp(-y^2), \tag{6.1}$$

and

$$f'(y,0) = 0 + \epsilon \exp(-y^2), \tag{6.2}$$

where the first terms on the right-hand sides are the steady solutions, $f'_{(steady)}[c](y)$ (the well-localized planar jet solution for each c) and 0 (trivial solution), and the second terms are the disturbances with ϵ being a constant representing their amplitudes. Next, in order to see a nonlinear coupling between g and f, we consider the initial conditions, (6.2) and

$$-g''(y,0) = \epsilon \exp(-y^2), \tag{6.3}$$

which respectively may be regarded as a localized planer jet and a localized vortex layer. The initial conditions (6.1), (6.2) and (6.3) satisfy the symmetries $f'(-y) = f'(y)$ and $g''(-y) = g''(y)$ and equations (2.5) and (2.6) are compatible with these symmetries so that the solutions for $t > 0$ also satisfy them.

In order to solve (2.5) and (2.6) numerically, it is convenient to introduce the rescaled variables η, J and H defined by $y = \tan\eta$, $J(\eta,t) = -g''(\tan\eta,t) = -g''(y,t)$ and $H(\eta,t) = -1 - f'(\tan\eta,t) = -1 - f'(y,t)$. Then the infinite domain $(-\infty,\infty)$ of y reduces to the finite domain $(-\pi/2,\pi/2)$ of η, and (2.5) and (2.6) can be written as

$$\frac{\partial}{\partial t}J - cJ + 2\cos^3\eta\sin\eta J' - \cos^4\eta J'' = \left(\int_0^\eta \frac{J(\zeta)}{\cos^2\zeta}\mathrm{d}\zeta\right) H'\cos^2\eta - \left(\int_0^\eta \frac{H(\zeta)}{\cos^2\zeta}\mathrm{d}\zeta\right) J'\cos^2\eta, \tag{6.4}$$

and

$$\frac{\partial}{\partial t}H - 2cH - H''\cos^4\eta + 2H'\cos^3\eta\sin\eta - H^2 + \left(\int_0^\eta \frac{H(\zeta)}{\cos^2\zeta}\mathrm{d}\zeta\right) H'\cos^2\eta + 1 - 2c = 0, \tag{6.5}$$

respectively, where the prime denotes differentiation with respect to η. The boundary conditions (2.3) and (2.4) can be read as $J(\pm\pi/2,t) = 0$ and $H(\pm\pi/2,t) = -1$. We discretize the η-space uniformly, and use the forward and the central difference approximations for time and spatial (η) derivatives, respectively, and trapezoidal quadrature for integrals in (6.4) and (6.5). The values of $H(\eta,0) = -1 - f'_{(steady)}[c](\tan\eta)$ at the mesh point in η-space can be evaluated by using a cubic-spline interpolation, in which we use the approximate values of $f'_{(steady)}[c](y)$ only in the range where f' behaves like a Gaussian (see § 3) and $f'_{(steady)}[c](\pm\infty) = 0$. In the computation, we fix the values of J and H at $\eta = \pm\pi/2$ to 0 and -1, respectively, and impose no other conditions on J and H except for their initial symmetries. Note that the well-localized solution $f'_{(steady)}[c](y)$ which behaves like $|f'| \sim A\mathrm{e}^{-y^2/2}|y|^{2c-3}$ for large $|y|$ and which is obtained for each value of $c > 0$, is consistent with (2.4) and $H(\pm\pi/2,t) = -1$, irrespectively of c. Note also that the steady solutions which are obtained for $c > 1$ and which behave like $|f'| \sim A|y|^{2-2c}$ for large $|y|$ are consistent with $H(\pm\pi/2,t) = -1$.

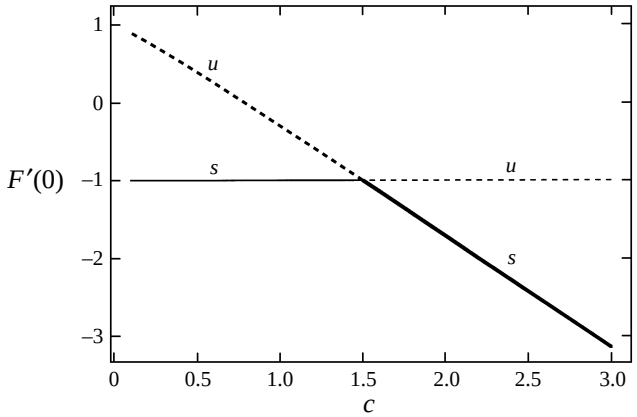

FIGURE 8. Plots of the values of $F'(0)$ listed in table 1 which are for $F'(y) = -1 - f'_{(steady)}[c](y)$ (thick line), as well as $F'(0) = -1$ which is for the trivial solution $F'(y) = -1$ (thin line) as functions of c. Solid lines indicate that the corresponding solutions are stable (s), and broken lines unstable (u).

Numerical results

Stability of the planar jet solution

The numerical solutions of (2.6) subject to the initial condition (6.1) behave as follows:

(i) for $0 < c < 1.5$, the solution with $\epsilon = 0.1$ converges asymptotically to $f' = 0$, while the solution with $\epsilon = -0.1$ grows exponentially in the negative f'-direction;

(ii) for $1.5 < c < 3.0$, both the solutions with $\epsilon = 0.1$ and -0.1 converge to a steady state whose value of $F'(0) = -1 - f'(0)$ is in good agreement with the one listed in table 1.

The solutions subject to (6.2) behave as

(iii) for $0 < c < 1.5$, both the solutions with $\epsilon = 0.1$ and -0.1 converge asymptotically to $f' = 0$;

(iv) for $1.5 < c < 3.0$, the solution with $\epsilon = 0.1$ converges to a steady state as described in (ii), while the solution with $\epsilon = -0.1$ grows exponentially in the negative f'-direction.

The numerical solution for $c = 2$ with $\epsilon = 0.1$ at its steady state described in (iv) is plotted in figure 3, which shows that the asymptotic solution for large t is in good agreement with the well-localized planar jet obtained in § 3. The Fourier spectrum of the converged solution described in (iv) behaves as $|f'(k)| \propto k \exp(-\alpha k)$ for large k, where α was confirmed to agree well with the value of $e^{p/2}$ listed for each $c \in (1.5, 3.0)$ in table 2.

The above results suggest that the inward planar jets, $f'_{(steady)}[c]$ for $0 < c < 1.5$, are unstable and the outward ones for $1.5 < c\,(< 3.0)$ are stable to the disturbances as in (6.1), while the trivial solution with no vorticities is stable for $0 < c < 1.5$ and unstable for $1.5 < c\,(< 3.0)$. The latter can also be shown by a linear analysis (see the Appendix). The results in this subsection can be summarized by a kind of 'bifurcation diagram' as shown in figure 8.

Coupling between g (vortex layer) and f (planar jet)

Since the existence of g does not affect (2.6), we have the same results regarding f as in (iii) and (iv) discussed above. On the other hand, the existence of f (planar

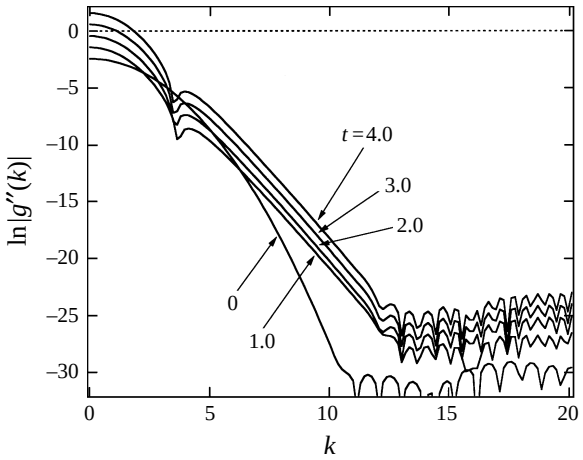

FIGURE 9. Plots of the Fourier transform $\hat{g}''(k,t)$ of $g''(y,t) = -G(y,t)$ obtained by solving numerically (6.4) and (6.5).

jet) may affect the evolution of g (vortex layer) through a nonlinear coupling on the right-hand side of (2.5). To see the effect of the nonlinear coupling with f, we first assume $f = 0$ and consider the stability of the trivial solution $-g'' = 0$ to the perturbation given by (6.3) with $\epsilon \ll 1$, and then proceed to the case of $f \neq 0$.

Substituting $f = 0$ into (2.5) and putting $G = -g''$, we have

$$\frac{\partial}{\partial t}G = M[G], \quad M[G] \equiv cG + G'' + yG' = 0. \tag{6.6}$$

Denoting the eigenvalue of M by μ, we have

$$\mu G - cG - G'' - yG' = 0. \tag{6.7}$$

Note that (6.7) is of the same form as (A 3). The general solution of (6.7) is therefore also a linear combination of u_e and u_o defined by (A 5) provided that $\sigma\,(= \lambda/2+3/2-c)$ in (A 5) is replaced by $\sigma = (\mu + 1 - c)/2$. Since the perturbation under consideration satisfies $g''(-y) = g''(y)$ and $|g'| = O(|y|^0)$ as $y \to \pm\infty$, the solution of (6.7) is required to satisfy $G(-y) = G(y)$ and $G(y) = o(|y|^{-1})$ for $|y| \to \infty$ as the boundary condition. As shown in the Appendix, these requirements lead to the inequality, $\mathrm{Re}(\mu)+1-c < 0$. This inequality implies that for $c < 1$ all the eigenvalues are negative so that $G \equiv 0$ is stable for $c < 1$, but positive eigenvalues may occur for $c > 1$. In fact, when $f = 0$, the behaviour of the numerical solution of (2.5) subject to the initial condition (6.3) with $\epsilon = 0.1$ is consistent with the linear analysis and the results are summarized as follows:

(v) for $0 < c < 1$, the vortex layer whose vorticity distribution is initially given by (6.3) converges to $-g'' = 0$;

(vi) for $c > 1$, the vortex layer $(-g'')$ grows exponentially in time.

Together with the results regarding f, it can be concluded that $-g'' = 0$ and $f' = 0$ are stable asymptotic solutions of (2.6) and (2.5) for $c < 1$. The behaviour of the numerical solutions subject to (6.3) and (6.2) with $\epsilon = 0.1$ is summarized as follows:

(I) for $0 < c < 1$, both the vortex layer $(-g'')$ and the vortex quadrapole $(-xf'')$ converge to $-g'' = -xf'' = 0$;

(II) for $1 < c < 1.5$, $-g''$ grows exponentially in time while $-xf''$ converges to $-xf'' = 0$;

(III) for $c > 1.5$, $-g''$ grows exponentially in time while $-xf''$ converges to $-xf''_{(steady)}[c]$.

The results (I)–(III) are consistent with (i)–(vi). Regarding the results (v) and (I), it should be noted that when $c < 1$ the rate of strain in the x-direction is stretching. The effect of the nonlinear coupling between f and g can be found in the spectrum of $-g''$ of the solutions in (III). It is shown in figure 9 that the spectra of $-g''$ for $t > 0$ decay exponentially with k for large k. Note that when $f' \equiv 0$, (2.5) has a solution which grows exponentially in time and whose spectrum is Gaussian-like all the time. The result implies that once the dynamics of the vortex layer ($-g''$) couples with that of the planar jet (f'), $-g''$ obeys a nonlinear equation and inherits the fine-scale structure of f'. It is clear that the origin of the small-scale structure in $-g''$ is the nonlinear coupling with f'.

7. Conclusions and discussion

A class of exact solutions of the Navier–Stokes equations is derived. Each of them provides a simple model of a thin vortical layer (a planar jet) under a uniform strain field $\boldsymbol{U} = (ax, by, cz)$ in three-dimensional infinite space. Unlike the well-known Burgers vortex layer or tube models, the nonlinear coupling between small eddies plays a key role in the dynamics governing the small-scale vortex structure in the model.

The thin vortical layer is represented as $\boldsymbol{u}(x, y) = (u, v, 0)$, so that the vorticity is parallel to the z-axes. It is assumed that $b < 0$ and $c > 0$, where $b < 0$ implies convection of the vortex lines towards the $y = 0$ plane and $c > 0$ vortex stretching in the z-direction (figure 1). In the present model, the thin vortical layer is expressed in terms of a stream function given by $\psi(x, y) = xf(y)$. This form reflects a scale separation of the velocity field, and may be justified when the characteristic scale in x is much larger than that in y. It is shown numerically that for each value of $\hat{c} \equiv c/|b| > 0$, there exists a steady solution which represents a well-localized planar jet under the uniform strain field. The small-scale structure of the flow field represented by the solution is studied by numerically analysing (i) the Fourier spectrum $\hat{u}(k)$ of the velocity field $u(y) = u(x, y)/x = f'(y)$ in § 4, (ii) the analytic structure of $u(y)$ in the complex y-plane in § 5, and (iii) the stability of the exact solutions (including a trivial solution $f' = 0$) in § 6. The results of (i)–(iii) may be classified according to the value of $\hat{c}$ and summarized as follows:

I. For $0 < \hat{c} < 1.5$

(i) Fourier spectrum $\hat{u}(k)$ for large k: exponential fall-off with an oscillation (figure 6);

(ii) analytic structure of $u(y)$: dominated by four poles of order 2 at $y = \pm a_1 \pm b_1 \mathrm{i}$;

(iii) stability: unstable (trivial one = stable).

II. For $\hat{c} > 1.5$

(i) Fourier spectrum $\hat{u}(k)$ for large k: exponential fall-off (figure 4);

(ii) analytic structure of $u(y)$: dominated by two poles of order 2 at $y = \pm b_2 \mathrm{i}$;

(iii) stability: stable (trivial one = unstable).

The values $a_1 + b_1 \mathrm{i} (= \xi)$ for $0 < \hat{c} < 1.5$ and $b_2 \mathrm{i} (= \mathrm{e}^{p/2}\mathrm{i})$ for $\hat{c} > 1.5$ are listed in table 2.

A simple analysis of the equation for $F(y) = -y - f(y)$ shows that the balance between the nonlinear and viscosity terms in the equation determines the dominant behaviour of F as $-6/(y - y_0)$ near a singularity at $y = y_0$. This is consistent with those

in (ii), which are obtained by analysing the Taylor expansion of $F(y) = -y - f(y)$ at $y = 0$. It is shown for case II that a function with singularities $-6/(y \pm b_2\mathrm{i})$ approximates well the function $F(y)$ near $y = 0$. Based on the singularity analysis in (ii), we have obtained asymptotic forms of the Fourier spectrum $\hat{u}(k)$ for large k as in (5.9) for case I and (5.8) for case II, where the exponential decay rates are given by b_1 and b_2, respectively. The spectra (5.9) and (5.8) show good agreement with those in I (i) and II (i), respectively. It is seen from these facts that nonlinearity plays a key role in the dynamics governing fine-scale structures characterized by the exponential decay of the spectrum of the velocity. Note that when $\psi = g(y)$, the equation for $g(y)$ is linear and the spectrum of the solution, such as Burgers vortex layer, is Gaussian-like as shown in § 2. The result II (iii) implies that the structure represented by the exact solution for $\hat{c} > 1.5$ may be realized as an asymptotic state of the time-dependent solution expressed in terms of the stream function given by $\psi(x, y, t) = xf(y, t)$.

The present vortical layer model is based on the assumption that the characteristic length scale in the x-direction is much larger than that in y, as implied in the expansion of the stream function ψ as in (2.2), or the approximation $\psi(x, y, t) = g(y, t) + xf(y, t)$. When the flow field is independent of x, then $f = 0$, i.e. $\psi = g$, and the governing equation, which is linear in $\psi = g$, has solutions which represent a vortex layer and such that for $\hat{c} > 1.0$, the amplitude of the vorticity $|g''(y, t)|$ grows exponentially in time while keeping a Gaussian-like spectrum for $t > 0$. However, the flow field in general depends on x, so that f is not zero. The governing equations for $\psi = g + xf$ are then nonlinear in g and f, but the equation for f is independent of g. Numerical computations in § 6 for the evolution of a vortex layer $(-g'')$ coupled nonlinearly with a vortex quadrapole $(-xf'')$ show that for $\hat{c} > 1.5$, the vortex layer grows exponentially in time while the vortex quadrapole tends to the steady state as in II (iii). The vorticity $-g'' - xf''$ for finite x is therefore dominated by the term $-g''$ and the f-term itself does not much contribute to the vorticity distribution, as compared to the g-term. However, it is also shown that the spectrum of such a coupled vortex layer $-g''(y, t)$, which is initially set to be Gaussian, starts to fall off only exponentially with k for large k. This fact implies that the existence of f, however small it may be, is crucial in the determination of fine-scale vortical structures. Once the x-dependence appears, the system becomes nonlinear, and the g-term, which dominates the total vorticity, inherits the fine-scale structure represented by the steady exact solutions of f studied in this paper. The results in § 6 suggest that the exact solutions as well as the fine-scale structures given in this paper are expected to arise where there is a scale separation in the distribution of vorticities under a certain strain field corresponding to $\hat{c} > 1.5$.

As mentioned above, when $g \neq 0$ and $\hat{c} > 1.0$, the vorticity grows exponentially in time. This is essentially due to the assumption that the background linear velocity field occupies an infinite space, and therefore the fine-scale structures represented by the present model are to be understood as *local* and *transient* ones (see the discussion in Monin & Yaglom, 1975, § 22.3). In this sense, the model provides one of the simplest prototypical local vortical structures which may occur in real turbulence, where not only the strain rates, the orientation of the vorticity and the rotational effect of the background velocity field, but also the configuration of the localized vortex sheets, tubes, etc., may vary randomly in time and space. It would be interesting to derive statistical quantities such as the energy spectrum of turbulence taking into account these factors and the model dynamics presented in this paper as one of the fundamental processes.

The authors are very grateful to Professor W. R. C. Phillips for valuable comments. We have also benefited from valuable comments by Professors D. W. Moore, H. Okamoto and S. J. Cowley. This work was supported in part by a Grant-in-Aid for Scientific Research from the Ministry of Education, Science, Sports and Culture of Japan, and by the Japan Society for the Promotion of Science.

Appendix. Linear stability analysis

As shown numerically in § 6, the trivial solution $F'(y) \equiv -1$ ($f'(y) \equiv 0$) is stable for $0 < c < 1.5$ and unstable for $c > 1.5$ to the perturbation given by (6.2). The following linear stability analysis shows that the stability of the solution $F' \equiv -1$ changes at $c = 3/2$.

Substituting $F'(y,t) = -1 - f' = -1 - u(y,t)$ into (2.9), we have the equation for u as

$$\frac{\partial}{\partial t}u + 2(1-c)u - u'' - yu' = u'\left(\int_0^y u(q,t)\mathrm{d}q\right) - u^2, \tag{A 1}$$

where we have used that f is an odd function of y. Here we consider perturbations which satisfy $u(-y) = u(y)$ and

$$\int_{-\infty}^{\infty} |u(q,t)|\mathrm{d}q < \infty, \tag{A 2}$$

like the one given by (6.2). (The condition $u \to 0$ as $|y| \to \infty$ is here necessary but not sufficient for (A 2).) Linearization of (A 1) with respect to u gives

$$\frac{\partial}{\partial t}u = L[u], \quad -L[u] \equiv 2(1-c)u - u'' - yu'.$$

Denoting the eigenvalue of the operator L by λ, we have

$$\lambda u + 2(1-c)u - u'' - yu' = 0. \tag{A 3}$$

The solution of (A 3) is here required to satisfy $u(-y) = u(y)$ and $u(y) = o(|y|^{-1})$ for large $|y|$ because of (A 2). Note that differently from (3.1), (A 3) is an equation for the entire range of y. With the substitution of $u = \mathrm{e}^{-y^2/2}w(y^2/2)$ into (A 3), we obtain the equation for $w(z)$:

$$zw''(z) + (1/2 - z)w'(z) = (\lambda/2 + 3/2 - c)w(z), \tag{A 4}$$

where the prime denotes differentiation with respect to $z(= y^2/2)$. The solution of (A 4) is a linear combination of the following even and odd functions:

$$w_e = M(\sigma, 1/2; z), \quad \text{and} \quad w_o = z^{1/2}M(\sigma + 1/2, 3/2; z),$$

where $\sigma = \lambda/2 + 3/2 - c$ and M is the confluent hypergeometric function. The solution of (A 3) can be therefore expressed as a linear combination of

$$u_e = \mathrm{e}^{-y^2/2}M(\sigma, 1/2; y^2/2) \quad \text{and} \quad u_o = \mathrm{e}^{-y^2/2}yM(\sigma + 1/2, 3/2; y^2/2). \tag{A 5}$$

From the asymptotics of the confluent hypergeometric function $M(a,b;z)$ for large z given in Abramovitz & Stegun (1964, Sec. 13.5), it follows that asymptotics of u_e and u_o for large $|y|$ are

$$u_e \sim |y|^{2\sigma-1}, \quad \sigma \neq 0, -1, -2, \cdots,$$
$$u_o \sim |y|^{2\sigma-1}, \quad \sigma + \tfrac{1}{2} \neq 0, -1, -2, \cdots.$$

In order that u_e satisfies (A 2), it is necessary that $2\sigma - 1 < -1$, which gives an inequality for the eigenvalue λ:

$$\mathrm{Re}(\lambda)/2 + 3/2 - c < 0.$$

This inequality implies that for $c < 3/2$, $\mathrm{Re}(\lambda)$ is negative, and for $c > 3/2$, $\mathrm{Re}(\lambda)$ may be positive. This suggests that $F'(y) \equiv -1$ is stable for $c < 3/2$. (This does not claim that $F'(y) \equiv -1$ is stable in the dynamics obeying the Navier–Stokes equation rather than the reduced equation (2.9), i.e. it does not exclude the possibility that there may exist modes that are unstable in the Navier–Stokes dynamics, but stable in the reduced dynamics represented by (2.9).)

REFERENCES

Abramowitz, M. & Stegun, I. A. 1965 *Handbook of Mathematical Functions*. Dover.

Batchelor, G. K. 1953 *Homogeneous Turbulence*. Cambridge University Press.

Batchelor, G. K. 1967 *An Introduction to Fluid Dynamics*. Cambridge University Press.

Brown, S. N. & Stewartson, K. 1965 On similarity solutions of the boundary-layer equations with algebraic decay. *J. Fluid Mech.* **23**, 673–687.

Buckmaster, J. 1973 Viscous-gravity spreading of an oil slick. *J. Fluid Mech.* **59**, 481–491.

Chen, S., Doolen, G., Herring, J. R., Kraichnan, R. H., Orszag, S. A. & She, Z. S. 1993 Far-dissipation range of turbulence. *Phys. Rev. Lett.* **70**, 3051–3054.

Falkner, V. M. & Skan, S. W. 1931 Some approximate solutions of the boundary-layer equations. *Phil. Mag.* **12**, 865–896.

Frisch, U. & Morf, R. 1981 Intermittency in nonlinear dynamics and singularities at complex times. *Phys. Rev.* A **23**, 2673–2705.

Kaneda, Y. 1993 Lagrangian and Eulerian time correlations in turbulence. *Phys. Fluids* A **5**, 2835–2845.

Kerr, R. M. 1990 Velocity, scalar and transfer spectra in numerical turbulence. *J. Fluid Mech.* **211**, 309–332.

Kida, S. & Murakami, Y. 1987 Kolmogorov similarity in freely decaying turbulence. *Phys. Fluids* **30**, 2030–2039.

Kraichnan, R. H. 1959 The structure of isotropic turbulence at very high Reynolds number. *J. Fluid Mech.* **5**, 497–543.

Lundgren, T. S. 1982 Strained spiral vortex model for turbulent fine structure. *Phys. Fluids* **25**, 2193–2203.

Magnus, W. & Oberhettinger, F. 1954 *Formulas and Theorems for the Functions of Mathematical Physics*. Chelsea.

Moffatt, H. K., Kida, S. & Ohkitani, K. 1994 Stretched vortices – the sinews of turbulence; large-Reynolds-number asymptotics. *J. Fluid Mech.* **259**, 241–264.

Monin, A. S. & Yaglom, A. M. 1975 *Statistical Fluid Mechanics*. MIT Press.

Murray, J. D. 1984 *Asymptotic Analysis*. Springer.

Novikov, E. A. 1961 Energy spectrum of turbulent flow of an incompressible fluid *Dokl. Akad. Nauk SSSR* **139**, 331–334.

Phillips, W. R. C. 1996 On a class of unsteady boundary layers of finite extent. *J. Fluid Mech.* **319**, 151–170.

Press, W. H., Flannery, B. P., Teukolsky, S. A. & Vetterling, W. T. 1988 *Numerical Recipes*. Cambridge University Press.

Pullin, D. I. & Saffman, P. G. 1993 On the Lundgren-Townsend model of turbulent fine scales. *Phys. Fluids* A **5**, 126–145.

Robinson, A. C. & Saffman, P. G. 1984 Stability and structure of stretched vortices. *Stud. Appl. Maths* **70**, 163–181.

Saffman, P. G. 1992 *Vortex Dynamics*. Cambridge University Press.

Saffman, P. G. 1968 Lectures on homogeneous turbulence. In *Topics in Nonlinear Physics* (ed. N. J. Zabusky). Springer.

Tatsumi, T. 1980 Theory of homogeneous turbulence. *Adv. Appl. Mech.* **20**, 39–133.

Townsend, A. A. 1951 On the fine-scale structure of turbulence. *Proc. R. Soc. Lond.* A **208**, 534–542.